Differential diffusion in low Reynolds number water jets

J. R. Saylor[a] and K. R. Sreenivasan
Mason Laboratory, Yale University, New Haven, Connecticut 06511

(Received 24 April 1997; accepted 21 January 1998)

Experimental data on differential diffusion between two species with large and quite disparate Schmidt numbers were obtained in a turbulent water jet by optically measuring the two species concentrations simultaneously. Experimental conditions were chosen so that the species were dilute and did not affect the water density thereby avoiding inertial effects. Differential diffusion was found to be significant in magnitude, even in the absence of these effects. Schmidt number ratios of 4 and 18 were considered. Differential diffusion was found to be statistically significant and to manifest at scales larger than the computed Batchelor scale. In some instances the concentration signal for the species with larger diffusivity was simply a blurred version of the other, while in other instances structures present in one signal were completely absent from the other. This second observation, presumably a more complex effect due to diffusion across velocity gradients, is discussed. © *1998 American Institute of Physics.* [S1070-6631(98)00105-6]

I. INTRODUCTION

The transport and mixing of scalar quantities in fluid flows is a frequently studied phenomenon. The effect of the dimensionless diffusion coefficient (Schmidt number in the case of species concentration and Prandtl number in the case of temperature) on the time evolution, physical structure and statistical characteristics of the passive scalar field in fluid flows represents an important part of the fluid mechanics literature. Much less studied is the instantaneous relationship between multiple scalars transported in a fluid flow. Physical systems rarely involve the transport of a single scalar quantity. In combustion and reacting flows, oceanographic flows, atmospheric flows, as well as in biological flows, a plethora of species are simultaneously transported. Frequently it is the instantaneous ratio or difference between two or more scalar quantities which determines important characteristics in such flows. For example in combustion and reacting flows, knowledge of the means and higher order moments of the reactant concentrations is not sufficient for predicting the rate of reaction. Rather, at any given location in the flow, it is the instantaneous concentrations of the reactants which determines the system reaction rate.

The diffusion coefficients of species in multi-component transport systems are, in general, not equal and therefore the concentration fields of these scalar quantities can evolve differently. For example two species A and B, initially comprising a homogeneous mixture (and therefore completely correlated, initially), which is introduced into a flow can evolve into concentration fields $c_A(\underline{x},t)$ and $c_B(\underline{x},t)$ which are different, due to differences in their diffusion coefficients. This process is termed differential diffusion (sometimes ''preferential diffusion''), and represents one mechanism by which initially correlated scalar quantities can become decorrelated in fluid flows. A brief review of the experimental and theoretical work on differential diffusion is now presented.

Within the field of combustion, many models rely on the assumption that differential diffusion is negligible. These models employ the so-called ''equal-diffusivity theory'' or ''conserved scalar approach.'' The assumption of equal diffusion coefficients among all species reduces the combustion problem from one governed by many coupled equations, each having a reaction source term, to one with a single equation without a reaction source term, greatly simplifying the modeling of reacting flows. Use of the conserved scalar approach is justified by arguing that, for large Reynolds numbers, the effect of molecular diffusion will only be observed in the high wave number end of the spectrum, and that means, variances, and covariances will be unaffected by differential diffusion.

The validity of this assumption at moderate and small Reynolds number has been questioned.[1–4] Experimental evidence exists which supports this concern for the validity of the conserved scalar model. Drake and co-workers[5,6] performed experiments in laminar, transitional, and turbulent diffusion hydrogen/air flames and observed deviations as large as 50% between measured concentrations and adiabatic equilibrium predictions for the laminar flame, which they attributed to differential diffusion. Bilger[2] developed a model for differential diffusion in a turbulent diffusion flame and applied it to the experimental conditions of Drake *et al.*[5] and obtained similar results. Bilger[1] recast the data of Tsuji and Yamaoka[7] for a methane diffusion flame and found differential diffusion effects as large as 18%. Evidence for the existence of differential diffusion in flames has also been observed by other researchers, for example Vranos *et al.*[8] in hydrogen/methane turbulent jet flames and Masri *et al.*[9] in hydrogen/carbon dioxide diffusion flames.

Nonreacting or ''cold'' flows have been used to study differential diffusion. Bilger and Dibble[3] numerically simulated a nonreacting jet consisting of a hydrogen/propane mixture at a Reynolds number of 2700. The variable z

[a]Current address: Naval Research Laboratory, Washington, DC 20375.

$$z=\zeta_i-\zeta_j, \tag{1}$$

was proposed to quantify differential diffusion effects between species i and j. Here

$$\zeta_i=\frac{Y_i-Y_{i2}}{Y_{i1}-Y_{i2}}, \tag{2}$$

Y_i is the mass fraction of species i and Y_{i1} and Y_{i2} are the mass fractions of species i in the nozzle fluid and surrounding fluid, respectively. The average value of z varied from a minimum of -0.005 to a maximum of 0.01, and the root-mean-square value (rms) of z varied from zero to a maximum of 0.004. Kerstein *et al.*[10] studied a nonreacting jet consisting of a hydrogen/Freon 22 mixture, having a nozzle Reynolds number of 20 000. The mean values for z were close to zero, while the rms of z was on the order of 0.05 in regions near the nozzle exit $(x/d=5)$. An important conclusion drawn from this work is that differential diffusion can have significant effects on species concentrations in flows, even for high (Re=20 000) Reynolds numbers.

Smith *et al.*[4] measured differential diffusion in a nonreacting turbulent jet, where the nozzle fluid consisted of a mixture of hydrogen and carbon dioxide, showing that the average value of z became negligible above a jet Reynolds number of 1000, while the rms of z was significant up to the largest Reynolds number investigated, Re=64 000.

Differential diffusion has also been investigated using numerical models. Kerstein has developed a linear-eddy model of turbulent transport and has applied it to differential diffusion,[10,11] and Yeung and Pope[12] have performed direct numerical simulations of differential diffusion in isotropic turbulence. Chen[13] simulated differential diffusion statistics in homogeneous turbulence.

In all of the experiments described above (both reacting and nonreacting) differential diffusion between two concentrated species was investigated. That is, the species under study are not dilute tracers being transported by a carrier gas, but rather comprise a large fraction (or all) of the flow. It is important to note several points with respect to this fact. First, concentrated mixtures of species having different densities can create density gradients as the process of differential diffusion proceeds.[14] Stated another way, differential diffusion between concentrated species can result in density gradients in a flow which initially had none. The swirling motions characteristic of many flows will act on such density gradients to separate the lighter species from the heavier ones. This effect is referred to as an ''inertial effect'' and the separation of species by this effect is referred to as ''inertial separation.'' (It should be noted that the term ''inertial effects'' sometimes refers to the deviation of particle paths from continuum streamlines in a particle-laden flow. Our use of this term pertains only to inertial separation of continuum species and not particles.) The presence of inertial effects in experiments designed to provide a better understanding of combustion is not necessarily bad, since inertial effects are certainly present in combustion systems. However, in other applications differential diffusion occurs where there are no inertial effects. For example, differential diffusion in environmental flows such as that which occurs between species such as ozone, carbon monoxide, NO_x, etc. downstream of a point sources of pollution is a dilute differential diffusion problem. This is also true of pollutant dispersal in water flows. Indeed, even in combustion, differential diffusion may occur between certain species which are dilute and where inertial effects are absent. Hence, experiments in the absence of inertial effects are needed for obtaining a better understanding of differential diffusion in dilute systems.

In addition to the practical need for understanding differential diffusion in dilute systems, a related, fundamental question needs to be addressed. Inertial separation of species acts to enhance differential diffusion. Hence, it is possible that in the experimental studies performed to date, differential diffusion acted to create a very small (perhaps unmeasurable) separation of species which was subsequently amplified to an observable level by inertial separation. The primary motivation of the present work is to address this point. Namely, does a significant and observable amount of differential diffusion exist in the absence of inertial effects, and if so, is there a difference in the characteristics of differential diffusion in a dilute system?

The second objective of this research was to determine qualitatively whether pure differential diffusion manifests only within diffusive length and time scales (i.e., the Batchelor scale), or on much larger scales. This is important since an argument in favor of equal-diffusivity modeling is that any difference in diffusion coefficients will have effects which are observable only at scales smaller than the characteristic diffusive scale. Hence, any indication that differential diffusion has effects on larger scales would warrant reconsideration of this assumption. While the notion of a Batchelor scale[15] is somewhat ambiguous in the low Reynolds number flow considered here, qualitative comparisons with the computed Batchelor scale can be made.

To address the points described above, we have investigated differential diffusion effects in a low-Reynolds-number turbulent jet where the nozzle-fluid consisted of a dilute, homogeneous mixture of two scalar species having substantially different diffusion coefficients. A jet was chosen for study because it is a classical flow with well-understood properties, and because it has frequently been used as an experimental and theoretical model for differential diffusion in combustion research. The concentration signals of the two species comprising the nozzle fluid have been measured simultaneously. To eliminate inertial effects we have considered a water flow where the species were fluorescent dyes, dissolved at extremely small concentrations. In the experiments presented herein, the presence of these dyes altered the fluid density by less than 0.001%, thereby eliminating the possibility of inertial separation. Because both species had the same boundary and initial conditions, any difference in the concentration fields of these two species was due solely to differential diffusion.

For this simple situation, the equation governing the transport of a passive scalar is

$$\frac{\partial c}{\partial t}=D\nabla^2 c-\underline{u}\cdot\nabla c, \tag{3}$$

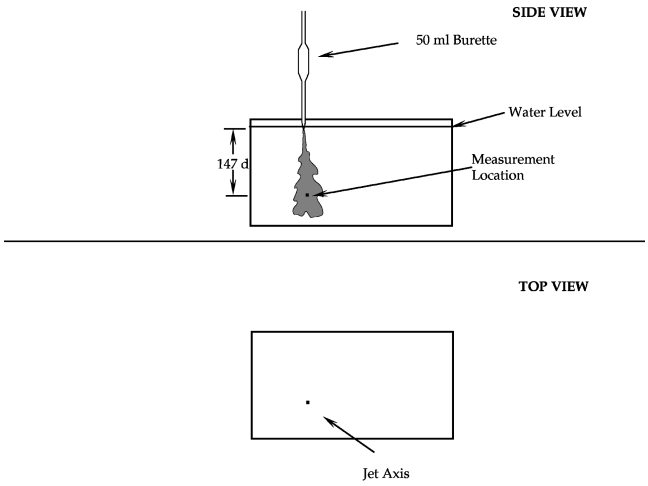

FIG. 1. Top and side views of jet setup.

where c is the species concentration, $\underline{u}$ the velocity vector, t time, and D the diffusion coefficient for the species. In dimensionless form Eq. (3) becomes

$$\frac{\partial C}{\partial T}=\frac{1}{\mathrm{Re\,Sc}}\nabla^2 C-\underline{U}\cdot\nabla C, \tag{4}$$

where $\underline{U}=\underline{u}/u_0$, $T=tu_0/d$ and $C=c/c^0$. Here u_0 is the nozzle exit velocity, d the nozzle diameter and c^0 the nozzle concentration; $\mathrm{Re}=u_0 d/\nu$ is the nozzle Reynolds number, ν is the kinematic viscosity of the fluid, and $\mathrm{Sc}=\nu/D$ is the Schmidt number.

Writing Eq. (4) for species C_1 and C_2 and subtracting one from the other, we obtain

$$\frac{\partial z}{\partial T}=\left[\frac{\nabla^2 C_1}{\mathrm{Pe}_1}-\frac{\nabla^2 C_2}{\mathrm{Pe}_2}\right]+\underline{U}\cdot(\nabla C_2-\nabla C_1), \tag{5}$$

where Pe is the Peclet number, $\mathrm{Pe}=\mathrm{Re\,Sc}$. Equation (5) demonstrates that the temporal changes of z, at any given location in the flow, is governed by Pe. It is noted that use of water as a carrier fluid renders the magnitude of the Peclet numbers used in this study much larger than those which are observed in combustion studies. This point will be further addressed in Section IV.

This paper is organized as follows; Section II contains details of the experimental methods. Sections III, IV and V describe, respectively, the results, their discussion and the conclusions reached from the study.

II. EXPERIMENTAL METHOD

A. Fluid dynamical aspects

The experiments described here were all done in a water jet. The jet emerged from a 50 ml glass burette with a nozzle diameter of 1.6 mm. As shown in Fig. 1, the jet entered a 35 liter water tank just below the water surface, and centerline measurements were made 147 nozzle diameters downstream. The nozzle exit velocity was 27 cm/sec, giving a Reynolds number $\mathrm{Re}=430$. The jet was gravity-fed and the head changed by about 1% during the course of an experimental run. The flow was allowed to come to steady state before data acquisition began. The jet was turbulent at the measurement station. Typical studies of turbulent jets employ Reynolds numbers which are larger than that chosen for this study. The relatively low Reynolds number was chosen here because of experimental constraints due to resolution of the small-scale structures in the flow. Since part of the motivation for performing these experiments concerns diffusion flames, it is worth noting that many laboratory flames are of low or moderate Reynolds number (e.g. Drake *et al.*[5]), and some are laminar (e.g. Tsuji and Yamaoka[7]).

TABLE I. Diffusion coefficients and Schmidt numbers in water for fluorescent dyes. A nominal viscosity for water of 10^{-6} m^2/s was used to compute Sc.

Dye	D (m^2/s)	Sc
Disodium Fluorescein	8.2×10^{-10}	1200
Basic Blue 3	2.3×10^{-10}	4400
Fluorescein Dextran	1.3×10^{-11}	77 000

The tank fluid was tap water filtered by a cellulose particle/rust filter (Aqua Pure AP124H/C) and an activated charcoal filter (Aqua Pure AP117) arranged in series. The jet fluid consisted of a dilute, homogeneous mixture of two fluorescing dyes dissolved in deionized water. Care was taken to ensure that the tank and jet fluid were at the same temperature so that natural convection did not occur. A solution of the fluorescent dye basic blue 3 (Sigma Chemical Co. 359.9 g/mole) was mixed with a solution of either disodium fluorescein (Fisher Scientific Co. 376.3 g/mole) or fluorescein dextran (Molecular Probes Inc. 70 000 g/mole) to create the nozzle fluid. The nozzle fluid concentrations were 5×10^{-5} moles/liter (M) for basic blue 3, 10^{-7} M for fluorescein dextran and 10^{-6} M for disodium fluorescein. For a few runs the fluorescein dextran concentration was 10^{-8} M and the disodium fluorescein concentration was 10^{-7} M. There was no difference between the results obtained from these runs and the regular runs. The diffusion coefficients and Schmidt numbers for all three dyes in water are given in Table I. The diffusion coefficient for disodium fluorescein was taken from the measurements of Quinn *et al.*[16] The diffusion coefficients for fluorescein dextran and basic blue 3 were obtained from the Stokes–Einstein estimation for a disk-shaped ellipsoidal molecule.[17]

The experiments were divided in two groups. In group I the jet fluid consisted of a dilute mixture of basic blue 3 and disodium fluorescein, giving a Schmidt number ratio of 4. In group II, a dilute mixture of fluorescein dextran and basic blue 3 was used, giving a Schmidt number ratio of 18.

B. Optical aspects

Measurements of the dye concentration were made by using laser induced fluorescence (LIF) techniques. The optical setup used for the measurements is shown in Fig. 2. The 488 nm line of an argon ion laser beam (Coherent, Innova 90) was used as the excitation source. The laser beam was reflected from a mirror and directed at an optical chopper which was used to pulse the laser, thereby minimizing the photobleaching of the dyes as will be discussed below. The

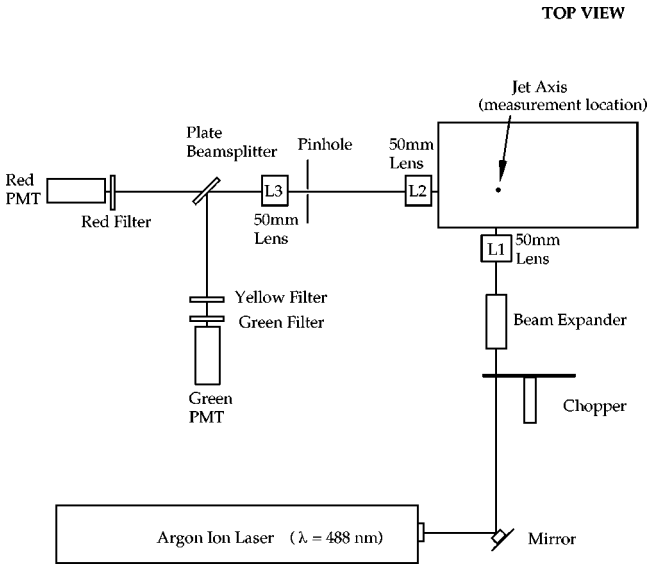

FIG. 2. Optical setup. See text for details.

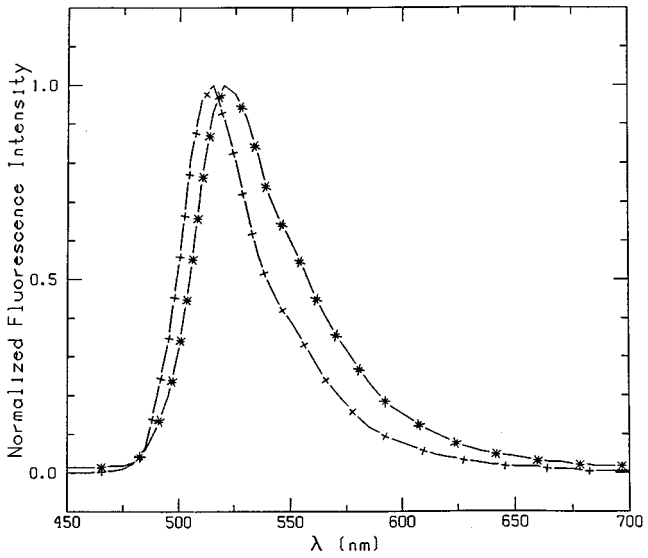

FIG. 3. Fluorescence intensity versus wavelength. -+- disodium fluorescein; -*- fluorescein dextran.

laser beam was expanded by a factor of 10 and subsequently focused by a 50 mm camera lens (L1) to a small volume at the measurement location within the jet. The fluorescent radiation emitted by the dyes in the measurement volume was collected by another 50 mm camera lens (L2) which focused the light onto a pinhole with a diameter of 300 μm. Light passing through the pinhole was collected and focused by lens L3. This light was split by a beam splitter so that the image of the pinhole was focused onto two identical photomultiplier tubes (Hamamatsu, R928). Optical filters were placed in front of the photomultiplier tubes (PMTs) so that the light corresponding to only one of the dyes was sensed by each PMT.

The dye fluorescence spectra were measured using a fluorescence spectrophotometer (Perkin-Elmer 650-40) with the excitation wavelength set at 488 nm. The spectra were repeatable and showed little variation with concentration for the levels used in the present experiments. The fluorescence spectra for disodium fluorescein and fluorescein dextran are plotted in Fig. 3. These spectra are virtually identical, having peaks separated by only 5 nm, and can be considered the same for present purposes. The fluorescence spectra for disodium fluorescein and oxazine-1 perchlorate (Eastman Kodak Co. 423.9 g/mole) are given in Fig. 4. Oxazine-1 perchlorate is optically identical to basic blue 3 and was used in a few preliminary experiments. However, its use was limited because of its prohibitive cost. The fluorescence emitted by fluorescein or fluorescein dextran was green in color and was recorded by one of the PMTs (to be designated the ''green'' PMT), while the fluorescence emitted by basic blue 3 appeared dark red in color and was recorded by the other PMT (the ''red'' PMT). Separation of these two signals was achieved using optical filters. A green short-wave-pass interference filter which blocked all red fluorescence, and a yellow glass filter which blocked all scattered laser light, were placed in front of the opening to the green PMT. A red glass filter which blocked green fluorescence as well as scattered laser light was placed in front of the red PMT. The transmission characteristics of these three filters, as obtained directly from the manufacturer, are superimposed with the dye fluorescence spectra in Fig. 4. Optical crosstalk was less than 1% of the primary signal.

The location of lens L2 (Fig. 2) with respect to the measurement volume and the pinhole was such that the image of the measurement volume was magnified by a factor of 9. The image of the waist of the laser beam, which comprised the measurement volume, fit completely within the diameter of the pinhole. Hence, the diameter of the laser beam at this point was less than 300 μm/9, or 33 μm. Assuming the cross-section of the laser beam at its waist to be circular, and using the fact that the pinhole itself is circular, one estimates that the measurement resolution is less than 33 μm in all directions.

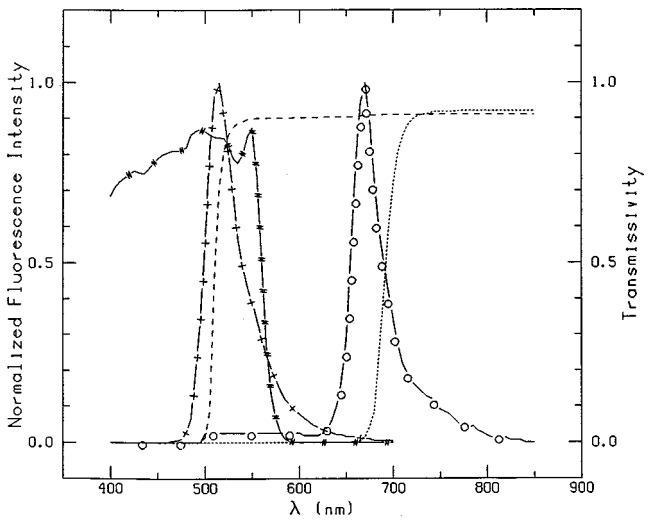

FIG. 4. Fluorescence intensity and transmissivity versus wavelength. -+- disodium fluorescein; -o- oxazine-1 perchlorate and basic blue 3; ... red filter; - - yellow filter; -#- green filter.

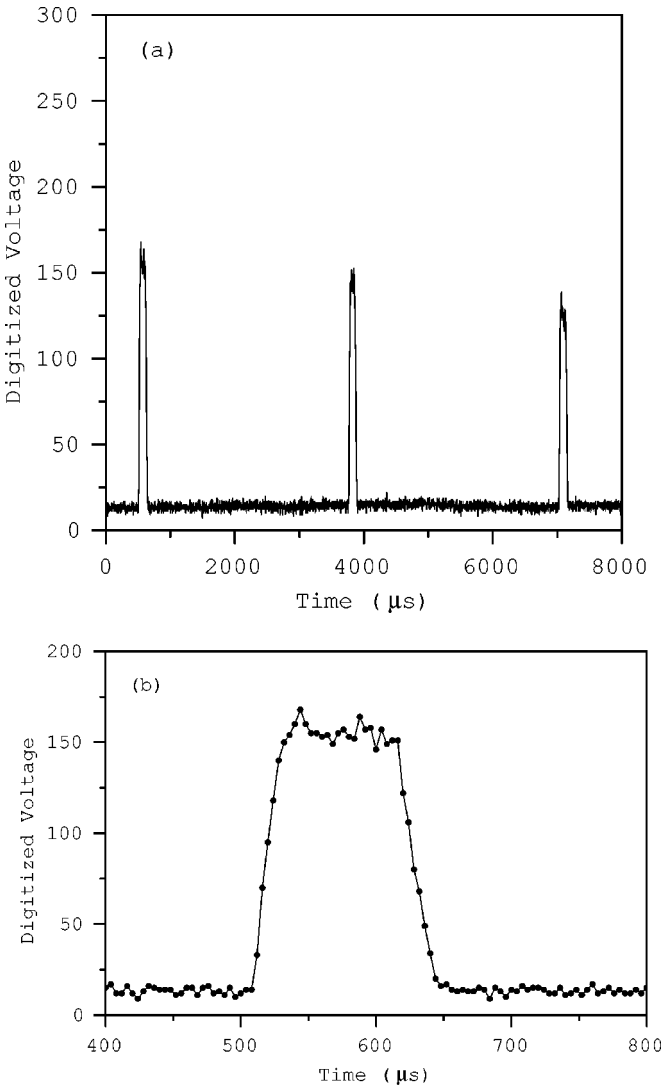

FIG. 5. Fluorescence pulses from the green channel of a sample jet run; (a) first three pulses from the sample run, and (b) magnified view of the first pulse.

C. Data acquisition and signal processing

Although the laser was pulsed, data were taken continuously at a rate of 250 kHz per channel for both channels. Consequently, the data file obtained during a run was actually a pulse train, with an inter-pulse space populated by the background. Within each pulse, the pulse height was proportional to the dye concentration. In Fig. 5(a), the first three pulses obtained from the green PMT during a sample jet run are presented along with a magnified view of the first pulse in Fig. 5(b). Each pulse consists of 32 points. To increase the signal to noise ratio, all points within each pulse were averaged. This averaging was done in post-processing mode by a program which identified the pulses by means of a user-defined threshold as a pulse identification criterion. The threshold was set to a level just above the noise floor. As a result of this conditional sampling, events where both channels had a zero-concentration signal, or a signal comparable in magnitude to the noise level, were not recorded. This did not affect the results since the concept of differential diffusion is not meaningful if there is no dye in the measurement volume.

D. Experimental errors

For the LIF experiments presented here, three major sources of error exists. These are photobleaching, fluorescence reabsorption (or ''trapping'') and nonlinearity in the fluorescence versus concentration characteristics. These three sources of error were investigated in detail and are described in Saylor;[14,18] they are recapitulated below.

Disodium fluorescein and fluorescein dextran are susceptible to photobleaching; this is the process by which constant irradiation of a dye molecule transforms it into a nonfluorescent state after a certain period of time. Photobleaching was insignificant for basic blue 3. The effect of photobleaching on the two green dyes was minimized by pulsing the laser for a period of time small enough to prevent a significant amount of photobleaching from occurring. These pulses were separated by a period of time, long enough so that the parcel of fluid in the laser focal region was convected downstream and did not receive a second pulse of laser light. For the experiments presented here, the laser pulse was 130 μs in duration and the inter-pulse interval was 3.2 ms.

The reabsorption of fluorescence emanating from the measurement volume, as it travels toward the collection optics, is another possible source of error. A detailed measurement of this error was performed and is described in Saylor.[14] In all cases, there were no observable trapping errors, meaning that these errors were smaller than the 2% overall system noise level.

Linearity of the fluorescence intensity versus dye concentration was also checked in detail (Saylor[14]) for all three dyes used. At sufficiently high concentrations, this plot will saturate, or flatten out. However, linearity was found to hold at the dye concentrations employed in these experiments.

III. RESULTS

Data were obtained from 28 jet runs in group I and 27 jet runs in group II. Each jet run lasted for one second during which 250 000 points were collected from each channel. As a result of the post-processing (which retained data only during the laser pulse and averaged within each pulse), about 300 processed data points resulted from each run. The exact number of data points varied slightly from run to run due to the nature of the conditional sampling described in Section II. A total of 6000 processed data points were obtained for the group I runs, and 8000 processed data points for the group II runs.

In Figs. 6(a), (b) the data from the green channel of a sample group I run are presented. The raw data for the green channel (disodium fluorescein) are plotted in (a), and the corresponding processed data in (b). The units of intensity for the raw data are volts from the PMT, digitized by the A/D converter. As already remarked, these voltages are linearly related to the dye concentration. From the processed

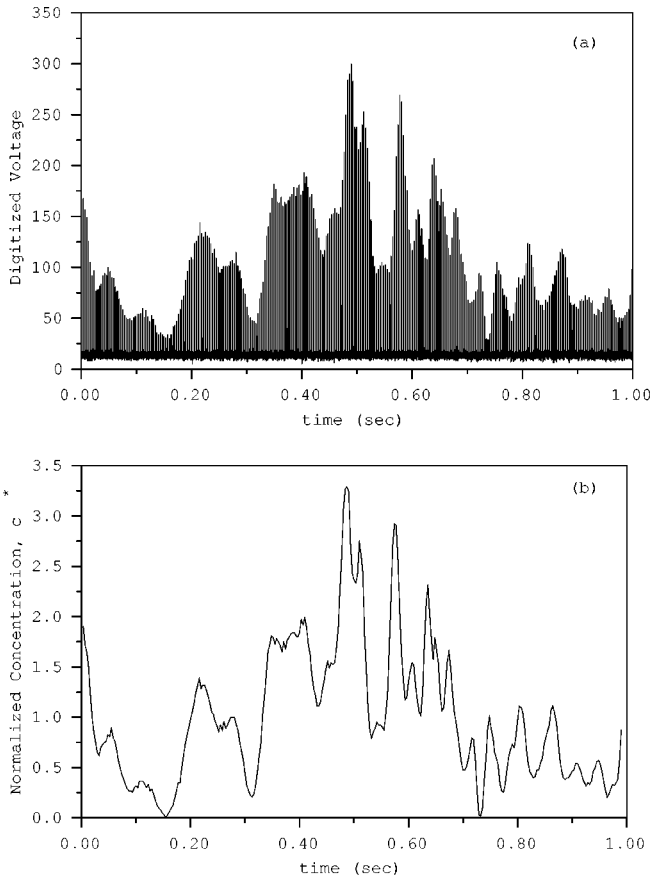

FIG. 6. (a) Raw data and (b) processed data for the green channel (disodium fluorescein) of a sample jet run.

data, a normalized concentration, c^*, was computed so that the signals from different runs and from both channels could be compared. c^* is defined as

$$c^* = c/\overline{c}, \tag{6}$$

where $\overline{c}$ is the average value of c for the run.

In Fig. 7 the processed data from a typical group I run and a typical group II run are presented. For each group, the green channel is presented on the left and the red channel on the right. The group I plots [Figs. 7(a), (b)] display similar behavior for the two channels, while the group II plots [Figs. 7(c), (d)] show that there is more small scale structure in the green channel than in the red channel. This is to be expected since fluorescein dextran is much less diffusive than basic blue 3, and hence should exhibit variations on much smaller scales; in the group I plots, for which disodium fluorescein and basic blue 3 have comparable Schmidt numbers, the differences between the green and red channels are smaller.

We define a variant of Bilger's[2] definition of the differential diffusion variable, z, by replacing ζ_i and ζ_j by c_G^* and c_R^*. That is,

$$z = c_G^* - c_R^*, \tag{7}$$

where c^* is defined in Eq. (6) and the subscripts G and R refer to the green and red channels, respectively. Figure 8 shows z for the first 250 data points of the runs presented in Fig. 7. The magnitude of z is clearly larger for group II [Fig. 8(b)] than for group I [Fig. 8(a)], and has non-zero values over many different scales. It should be noted that the total system noise level of 2%, indicated by the dotted lines in Figs. 8(a), (b) is much smaller than the magnitude of z observed, and cannot account for the observed behavior. These data show that, even in the absence of inertial effects, differential diffusion can be significant.

Part of the motivation for the present work was to determine whether differential diffusion occurs only at scales comparable to the diffusive length scale, or whether it can also exist at larger scales. Hence, it is desirable to make a comparison between the size of the z-structures seen in Fig. 8, and the Batchelor scale, η_b. Following Smith *et al.*,[4] we define η_b as

$$\eta_b = 0.38C(x - x_0)\mathrm{Re}^{-3/4}\mathrm{Sc}^{-1/2}, \tag{8}$$

where C is an experimentally determined constant. It should be noted that estimates of η_b are fraught with uncertainty since η_b depends on many factors, such as radial location in the flow and the assumptions made in estimating energy dissipation. Sreenivasan and Meneveau[19] point out that estimating these scales to within a factor of 2 is probably not appropriate. Specifically, values of the constant C in Eq. (8) have been found to vary dramatically. Dowling[20] obtained a value of $C = 2.5$, while Dowling and Dimotakis[21] report a value of $C = 12.5$. Sreenivasan and Prasad[22] use a value of unity, all for the case of a turbulent jet. In regard to the experiments presented here, the Reynolds number is relatively low, and hence the turbulence is probably not fully developed, further complicating the estimation of η_b.

In spite of these uncertainties, estimates of η_b were made so that a qualitative comparison between a characteristic diffusion length scale and the length scales observed in the z data obtained in the present work could be made. Following Sreenivasan and Prasad,[22] a value of unity was chosen for C. The effect of the uncertainties in C on the results is discussed below.

Using Eq. (8), the estimated Batchelor scales for disodium fluorescein, basic blue 3 and fluorescein dextran are 26 μm, 14 μm, and 3 μm respectively. Invoking Taylor's frozen flow hypothesis to convert the estimated Batchelor scales into time scales, one obtains time scales of 2.0 ms, 1.1 ms and 0.3 ms, respectively. The sample z-trace presented in Fig. 8(b) displays structures which are frequently greater than η_b. For example, the structure indicated in Fig. 8(b) is 26 times the larger Batchelor scale (for basic blue 3) and 97 times the smaller Batchelor scale (for fluorescein dextran), which is equivalent to 0.4 times the Kolmogorov scale for the flow. It is noted that the use of Taylor's frozen flow hypothesis in this low Reynolds number jet renders this comparison somewhat course. Nevertheless the very large difference between the observed differential diffusion scales and the Batchelor scale (e.g. a factor of 97 in the example noted above), probably exceeds the uncertainties due to Taylor's frozen flow hypothesis, as well as any concerns about estimates of the Batchelor scale, addressed earlier. For example, the variation in reported values for C (from 1 to 12.5) in Eq. (8), cannot account for the large sized z-structures. Moreover, in the group II data, for example, z-structures which

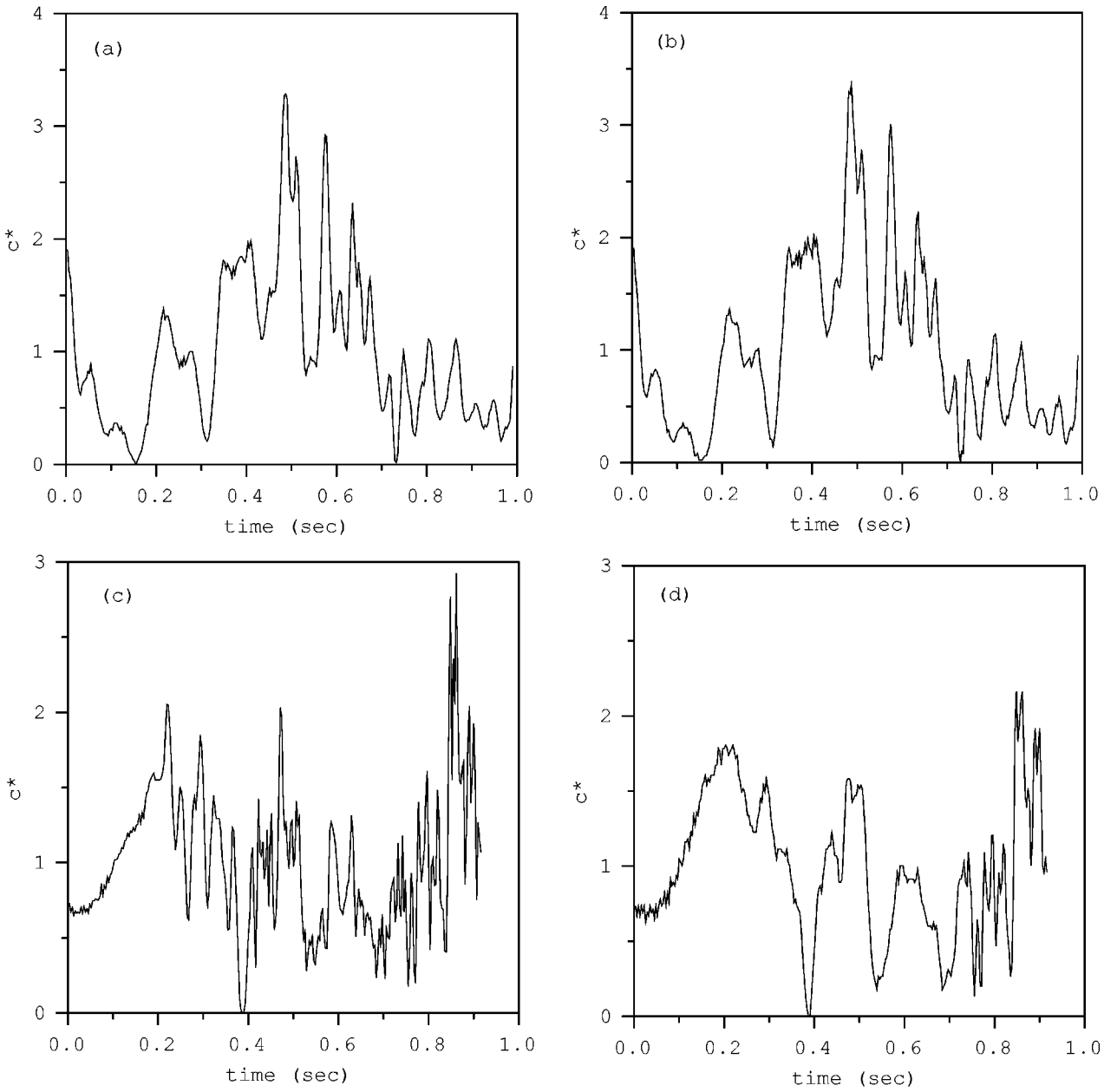

FIG. 7. Green and red signals for a Schmidt number ratio of 4 (a, b) and 18 (c, d). Green signals are plotted on the left, red on the right.

were 50 times the larger Batchelor scale were common, and even larger values were also observed. These data indicate that the diffusive separation of the two species is being spread to much larger scales by the convection. In this way, diffusion has a distinctly non-local effect on the concentration field. This will be discussed in further detail in the following section.

The z time traces for all runs were compiled, and a probability density function (pdf) was computed for both cases. The pdfs for the two cases are presented in Figs. 9(a), (c). The pdf for group I [Fig. 9(a)] is narrower and taller than that for group II [Fig. 9(c)]. For both cases the peak in the pdf is located at $z=0$ (which is also the average value for z in both data groups). The pdfs have a slightly jagged appearance, which would probably disappear with a larger data set. Convergence was tested by recomputing the pdfs using sequentially smaller subsets of the total data set. There was no significant change in the pdfs until less than 40% of the data was used. Semi-log plots of the group I and group II pdfs are presented in Figs. 9(b), (d). Included in both figures is a Gaussian having the same standard deviation as the experimental data. The agreement between the pdf for the experimental data and the Gaussian is reasonable. In Table II, the maximum, minimum and rms values for z are tabulated for both groups of data. All these measures of differential diffusion are larger for the group with the larger Schmidt number ratio. The contribution of noise to the rms values of z is the total system noise of 2%. This corresponds to an uncertainty in z_{rms} of 18% in group I and 7% in group II. This uncertainty does not explain the large values of z observed, nor the differences between z_{rms} for group I and group II.

A compilation of the processed data is presented in Fig.

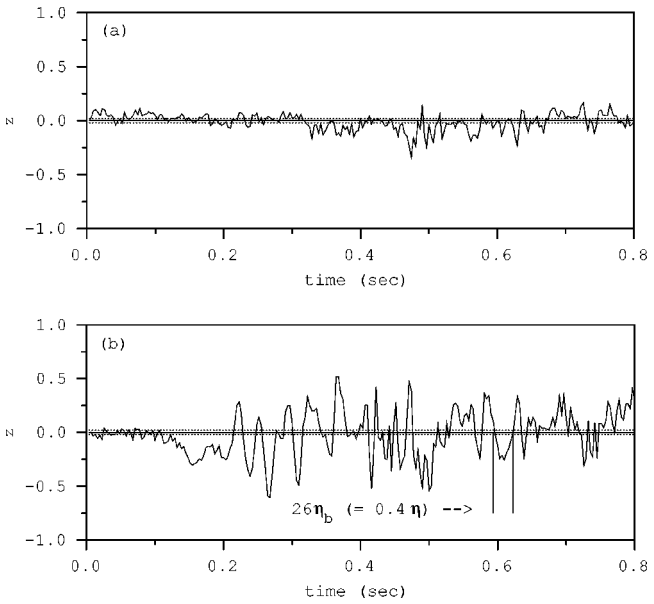

FIG. 8. Sample z traces for Schmidt number ratio of (a) 4 (group I) and (b) 18 (group II). The magnitude of the system noise is indicated. The size of a sample structure is indicated in (b) in terms of the Batchelor scale, η_b for basic blue 3 and for the Kolmogorov scale, η, of the flow. The two dotted lines in (a) and (b) bracket the total system noise.

10 in the form of scatter plots where the green channel data are plotted against the red channel data for each instant of time. The group I data [Fig. 10(a)] were better correlated than the group II data [Fig. 10(b)]; the former data have a correlation coefficient of $\rho=0.97$, while the latter have a correlation coefficient of $\rho=0.85$. Perfect correlation between the two channels ($\rho=1.0$) would have resulted in all points falling on the 45° line.

Because diffusion can occur only in the presence of gradients, a comparison of the gradients of the species is appropriate. In Fig. 11 the temporal gradients of the green and red channels are plotted against each other [Fig. 11(a) for group I data and Fig. 11(b) for group II data]. The correlation is better for the former (correlation coefficient is 0.91) than for the latter (correlation coefficient is 0.71).

IV. DISCUSSION

We found that the variable z, which quantifies differential diffusion was significantly different from zero. As shown in Table II, the rms of z was 0.1 for the group I data and 0.3 for the group II data. This demonstrates that, even in the absence of inertial effects, significant and observable differential diffusion can occur for Schmidt number ratios as small as 4. Visual comparison of the green and red channel signals in group II measurements revealed both local diffusive behavior (one channel being a blurred version of the other) and non-local behavior (structures present in only one of the channels). These results are discussed in some detail below.

We chose to normalize our concentration data to the local average, $\overline{c}$, while Kerstein *et al.*[10] and Bilger and Dibble,[3] normalized to the jet nozzle concentration, c^0. Appropriate comparison, therefore, requires a renormalization of the data. The work of Becker *et al.*[23] shows that the ratio $c^0/\overline{c}$ is insensitive to the dimensionless diffusion coefficient (either the Schmidt number or the Prandtl number) and is well correlated by the relation

$$\frac{c^0}{\overline{c}}=\frac{0.185[x-2.4d]}{d}, \tag{9}$$

where x is the downstream distance from the nozzle exit. Because $c^0/\overline{c}$ is not a function of the Schmidt number, dividing z and $z_{\rm rms}$ by $c^0/\overline{c}$ renormalizes them to the nozzle fluid concentration. For our experimental conditions Eq. (9) yields $c^0/\overline{c}=26.8$. The constants employed in Eq. (9) are not universal and their exact values will probably differ for the jet used here. However, for the purpose of comparing the present $z_{\rm rms}$ results to those of other authors, use of Eq. (9) is thought to be appropriate, especially in light of the order of magnitude variation in $z_{\rm rms}$ from author to author. The renormalized values are presented in Table III, along with those due to Kerstein *et al.*,[10] Bilger and Dibble,[3] and Smith *et al.*,[4] and are referred to as $z'_{\rm rms}$. The $z'_{\rm rms}$ values obtained for both groups of data are smaller than those of Kerstein *et al.*[10] The group I values are comparable to those of Bilger and Dibble,[3] and the group II values are comparable to those of Smith *et al.*[4]

No obvious trend or functional relationship between $z'_{\rm rms}$ and Pe, Re, x/d or $\mathrm{Sc}_1/\mathrm{Sc}_2$ follows from the data compiled in Table III. The results of Smith *et al.*[4] showed a decrease in $z'_{\rm rms}$ with increasing Re, at a given location in the flow. Since their experiments were done with constant Schmidt numbers, this implies a decrease in $z'_{\rm rms}$ with increasing Pe as well. For the experiments presented here, when Pe increased by almost a factor of 4, $z'_{\rm rms}$ actually increased, indicating that $z'_{\rm rms}$ is affected by more than just the Peclet number. While the form of Eq. (5) seems to indicate that Pe_1 and Pe_2 are the only dimensionless groups which affect this phenomena, it must be noted that Eq. (5) provides $\partial z/\partial T$ given local values for the gradients and Laplacians of both species, as well as the local velocity. Most likely, Pe and $\mathrm{Sc}_1/\mathrm{Sc}_2$, as well as the turbulence characteristics of the flow significantly affect $z'_{\rm rms}$, and a detailed parametric study is necessary to ascertain the appropriate functional relationships between the relevant dimensionless groups.

The Schmidt numbers and Peclet numbers investigated in these experiments are large, when compared to those of typical gas phase flows. To some degree this limits the relevancy of the current results to combustion. However, it should also be noted that the Schmidt number ratio, $\mathrm{Sc}_1/\mathrm{Sc}_2$ for these experiments is comparable to those of gas phase experiments (Table III), and indeed our values of $z'_{\rm rms}$ fall within the range of those obtained in gas phase differential diffusion experiments. What the experiments presented herein have demonstrated is that even in the absence of inertial effects, differential diffusion exists and is statistically significant. This has been demonstrated for large values of Pe only and it is theoretically possible that this conclusion will not hold at smaller values of Pe or Sc. It is our opinion that this possibility is remote, and suspect that a large change in any one of the parameters tabulated in Table III will sim-

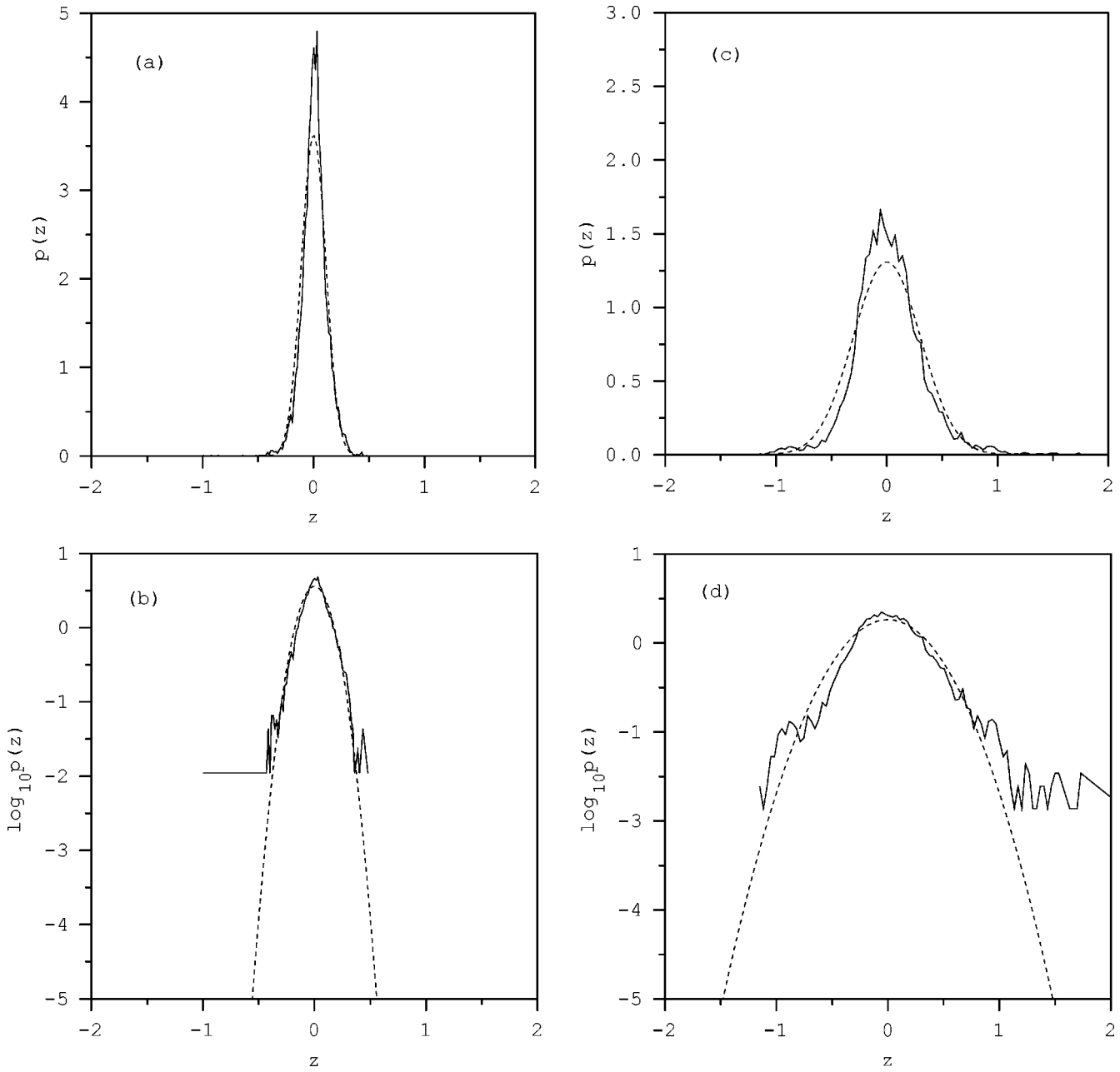

FIG. 9. PDFs for Schmidt number ratios of 4 (group I, (a, b)) and 18 (group II, (c, d)). (b) and (d) are semi-log plots of the data. A Gaussian having the same standard deviation as the PDF is included in each plot.

ply shift the location in the parameter space where significant z'_{rms} values will be observed. For example, in reducing $\mathrm{Sc}_1/\mathrm{Sc}_2$, one may have to travel further downstream (increase x/d) in order to observe large values for z'_{rms}. Again, a more detailed study is necessary to ascertain these functional relationships.

TABLE II. Schmidt number ratio, $z_{\max}$, $z_{\min}$ and z_{rms} for group I and group II runs.

	Group I	Group II
$\mathrm{Sc}_1/\mathrm{Sc}_2$	4	18
$z_{\max}$	0.478	2.13
$z_{\min}$	−1.01	−1.18
z_{rms}	0.110	0.305

Increasing Re and/or Sc decreases the scale at which diffusion acts to smooth out the scalar fluctuations. This fact has been used as an argument for ignoring differences in the species diffusion coefficients in combustion modeling.[2] The crux of this assumption is that diffusion effects in the concentration field exist only at diffusive scales. To better characterize the time scale over which differential diffusion acts, we computed the distance between zero crossings, Λ_z, in each z-trace and then computed an average distance between zero crossings, $\overline{\Lambda}_z$, for the group I and group II data. Events where z is non-zero and large for long periods of time indicate that diffusion is creating differences in the concentration

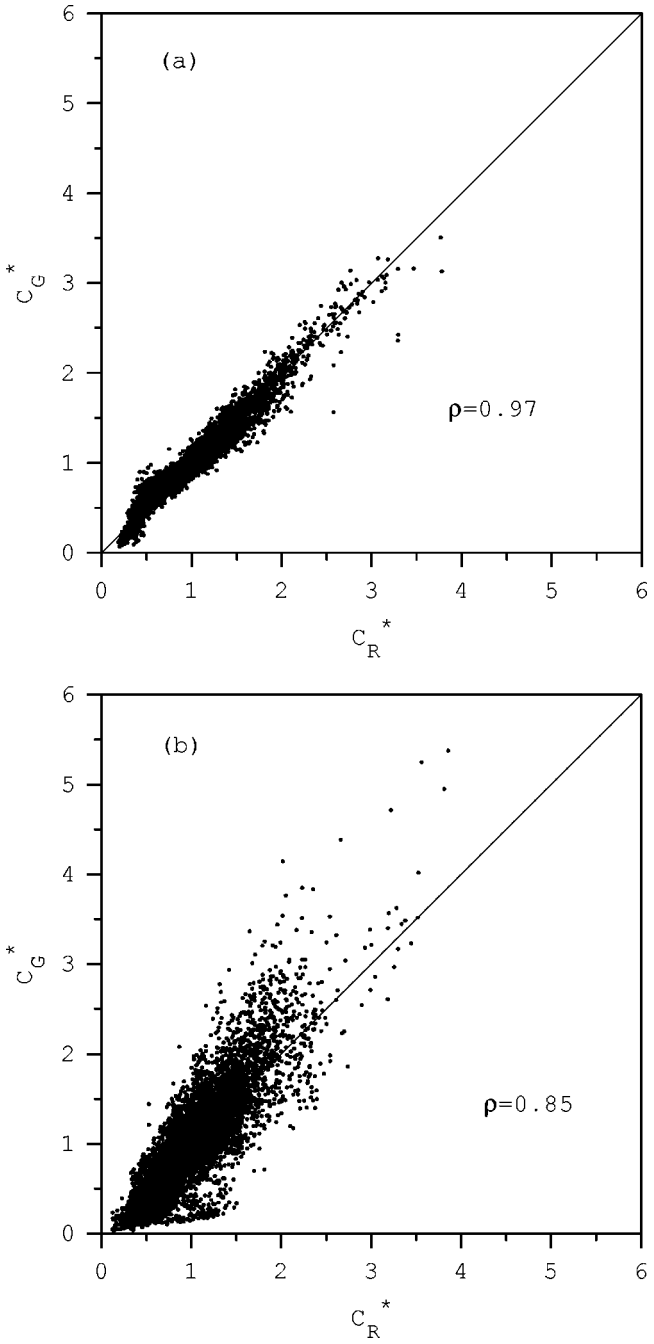

FIG. 10. Green channel versus red channel for (a) group I and (b) group II.

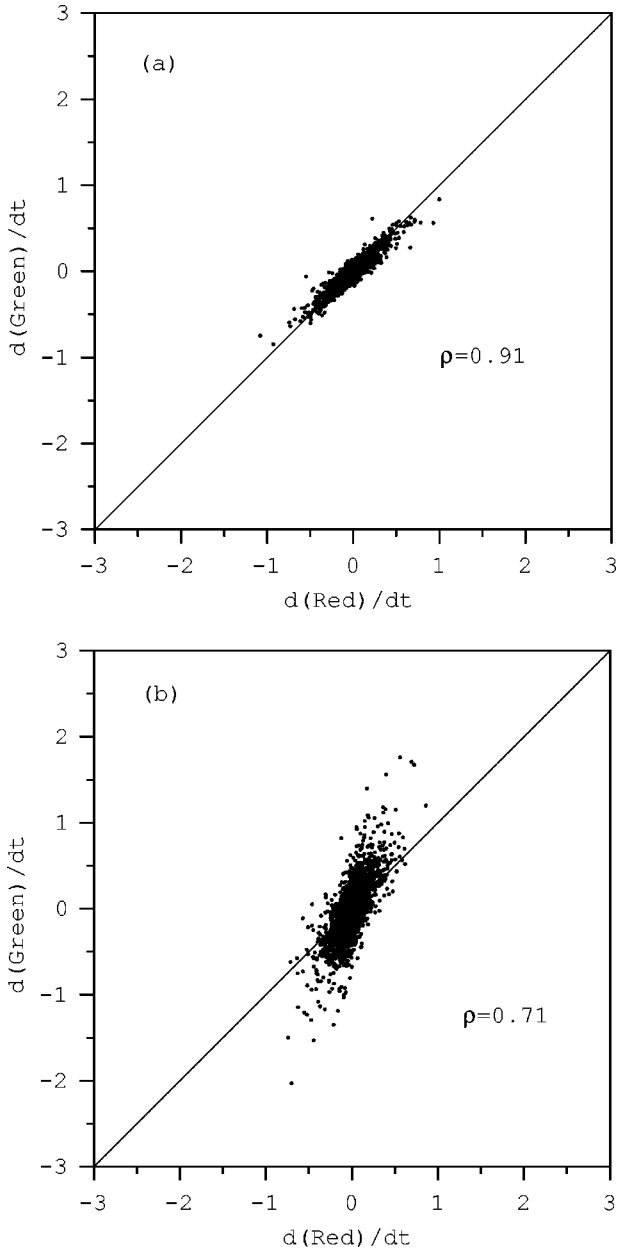

FIG. 11. Temporal gradient of green channel versus temporal gradient of red channel. (a) Group I data; (b) group II data.

signals over large spatial extent (again, invoking Taylor's frozen flow hypothesis). For example, if Λ_z is larger than η_b, then diffusion has had an effect over a scale larger than the diffusive scale. To reduce the influence of noise in this analysis, we considered zero crossings between which an extremum of $|z|>0.1$ existed. $\overline{\Lambda}_z$ was 19 ms for group I and 18 ms for group II, the former being 17 times the Batchelor scale. While some of the difference between $\overline{\Lambda}_z$ and η_b can be explained by the variation in the constant C in Eq. (8), it should be noted that $\overline{\Lambda}_z$ is an *average* of all the zero crossings. For the group II data, instances where Λ_z was 50 times the estimated Batchelor scale were common. And even for the smaller Schmidt number ratio group I data, values of Λ_z greater than 30 times η_b were common. In some cases, Λ_z was greater than the Kolmogorov scale. It would be difficult to explain these results by the uncertainties in C alone. Rather, one would have to conclude that diffusive effects are spilling over to the large scales. While it is not possible to make statements about all turbulent flows from this study of a very specific type of flow, it is important to note that the results contradict the general assumption that differential diffusion manifests only at scales smaller than the diffusive scales.

Manifestations of differential diffusion at scales larger than the diffusion scale are not without experimental support from other researchers. Long[24] presents image data obtained from a H_2/CH_4 jet entering an ambient air environment. Differential diffusion between H_2 and CH_4 resulted in measur-

TABLE III. z'_{rms}, Pe, Re, x/d and Sc_1/Sc_2 for the present work and from previous authors. The Peclet number, Pe, has been defined using the smaller Schmidt number of the two species. All values taken at the jet centerline.

Authors	z'_{rms}	Pe	Re	x/d	Sc_1/Sc_2
Kerstein *et al.*	0.025	4980	20 000	10	9
Bilger and Dibble [a]	0.003	1710	2650	10	15
Smith *et al.*	0.01	1320	8000	60	5
Present data (group I)	0.004	516 000	430	147	4
Present data (group II)	0.011	1.9×10^6	430	147	18

[a]Computational results.

able changes in the Rayleigh scattering signal which was recorded in the form of rectangular images. Typical images showed differential diffusion across scales on the order of 2 mm in a 4700 Reynolds number jet. This corresponds to a scale whose extent is about 100 Batchelor scales for CH_4 (about 125 Batchelor scales for H_2), results which are not dissimilar from those presented here.

When planning the present experiments, two mechanistic models were used to anticipate how differences in the passive scalar field might manifest as a result of differential diffusion. In the first model, model A, we imagined that differential diffusion would manifest at scales of the order of the Batchelor scale only: larger scales would look essentially identical for both dyes, the only difference being that the structures would be sharper for the high Schmidt number dye than for the low Schmidt number dye. At larger scales, say those much larger than the Batchelor scale, no differences would be observed. For model B, we imagined that a blob of the dye mixture, located at the edge of a Kolmogorov-scale sized eddy (say) would diffuse across the velocity gradient, into an adjacent eddy. If one of the dyes diffused preferentially into this eddy, the second eddy would contain both dyes, but the normalized dye concentrations would be unequal. Subsequent convection would stretch this region, resulting in differences in the passive scalar fields across scales larger than the Kolmogorov scale.

Support for both models exists in the data. In Fig. 12 a plot of the data from both channels of a sample group II run is presented. Two structures labeled ''A'' in the figure, illustrate how the low Schmidt number signal (b) is simply a blurred or smoothed version of the high Schmidt number signal (a), indicating a local diffusive effect. The regions labeled ''B,'' on the other hand, contain structures which exist in one channel, but not in the other. This, along with the zero-crossing results presented above, demonstrates that diffusion across a velocity gradient has a significant, non-local effect on the concentration field in this turbulent flow.

Finally, it must be noted that a better understanding of the differential diffusion effects calls for spatial data of the sort obtained by Kerstein *et al.*,[10] and Long *et al.*[24] We have obtained similar data for the present jet described, but for smaller x/d values. Although these images revealed significant differential diffusion at various scales, there was no evidence of model B behavior in the preliminary data examined to-date. We speculate, however, that the model B behavior will become more dominant at larger downstream distances.

V. CONCLUSION

To the best of our knowledge, the experiments presented here are the first studies of differential diffusion performed in the absence of inertial effects as well as the first experiments done in a liquid flow. We have shown that differential diffusion can be significant and observable in the absence of inertial effects for Schmidt number ratios as small as 4. Differential diffusion was observed over a fairly wide range of scales. Our measurements in a jet of Reynolds number 430, taken 147 diameters downstream of the nozzle, yielded $z_{rms} = 0.11$ when the Schmidt number ratio was 4 and $z_{rms} = 0.31$ when the Schmidt number ratio was 18. When appropriately renormalized, these values can be compared to those of Kerstein *et al.*,[10] Bilger and Dibble[3] and Smith *et al.*[4]

We found that z could be significant in magnitude over relatively large scales. These scales were found to frequently be larger than the estimated Batchelor scale, even taking into account the uncertainties in the estimation of the Batchelor

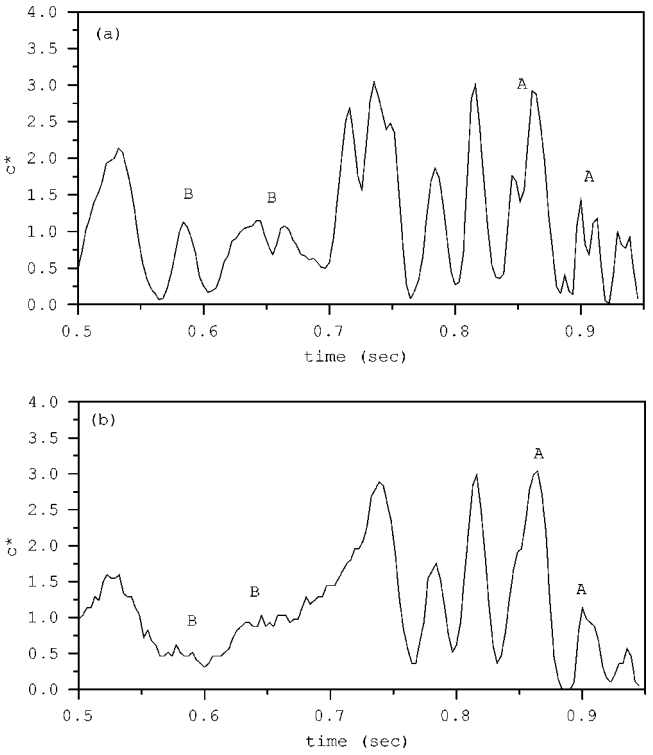

FIG. 12. Sample run for group II. (a) Green channel (fluorescein dextran); (b) red channel (basic blue 3).

scale. In specific instances, nonzero values for z existed over scales larger than the Kolmogorov scale for the flow.

We conclude that model B behavior (molecular diffusion across velocity gradients) may cause equal-diffusivity theory predictions to fail. This behavior coexists with a strong element of local diffusion (model A). Further work will be required to determine whether or not model B behavior dominates at higher Reynolds number.

ACKNOWLEDGMENTS

The authors thank Marshall Long for his advice and helpful suggestions and Robert Bilger, Gustavo Stolovitzky, Kevin Lyons and Jonathon Frank for helpful discussions. Financial support was provided by AFOSR.

[1]R. W. Bilger, ''Reaction rates in diffusion flames,'' Combust. Flame **30**, 277 (1977).
[2]R. W. Bilger, ''Molecular transport effects in turbulent diffusion flames at moderate Reynolds number,'' AIAA J. **20**, 962 (1982).
[3]R. W. Bilger and R. W. Dibble, ''Differential molecular diffusion effects in turbulent mixing,'' Combust. Sci. Technol. **28**, 161 (1982).
[4]L. L. Smith, R. W. Dibble, L. Talbot, R. S. Barlow, and C. D. Carter, ''Laser Raman scattering measurements of differential molecular diffusion in nonreacting turbulent jets of H_2/CO_2 mixing with air,'' Phys. Fluids **7**, 1455 (1995).
[5]M. C. Drake, M. Lapp, C. M. Penney, S. Warshaw, and B. W. Gerhold, ''Measurements of temperature and concentration fluctuations in turbulent diffusion flames using pulsed Raman spectroscopy,'' Eighteenth Symp. (Intl.) on Combustion, 1521 (1981).
[6]M. C. Drake, R. W. Pitz, and M. Lapp, ''Laser measurements on nonpremixed H_2-air flames for assessment of turbulent combustion models,'' AIAA J. **24**, 905 (1986).
[7]H. Tsuji and I. Yamaoka, ''Structure analysis of counterflow diffusion flames in the forward stagnation region of a porous cylinder,'' Thirteenth Symp. (Intl.) on Combustion, 723 (1971).
[8]A. Vranos, B. A. Knight, W. M. Proscia, L. Chiappetta, and M. D. Smooke, ''Nitric oxide formation and differential diffusion in a turbulent methane-hydrogen diffusion flame,'' 24th Symp. (Intl.) on Combustion (1992).
[9]A. R. Masri, R. W. Dibble, and R. S. Barlow, ''Chemical kinetic effects in nonpremixed flames of H_2/CO_2 fuel,'' Combust. Flame **91**, 285 (1982).
[10]A. R. Kerstein, R. W. Dibble, M. B. Long, B. Yip, and K. Lyons, ''Measurement and computation of differential molecular diffusion in a turbulent jet,'' International Symposium on Turbulent Shear Flows (7th) (1989).
[11]A. R. Kerstein, ''Linear-eddy modeling of turbulent transport. Part 3. Mixing and differential molecular diffusion in round jets,'' J. Fluid Mech. **216**, 411 (1990).
[12]P. K. Yeung and S. B. Pope, ''Differential diffusion of passive scalars in isotropic turbulence,'' Phys. Fluids A **5**, 2467 (1993).
[13]J. H. Chen, ''Differential diffusion statistics in homogeneous turbulence,'' Fourth International Conference on Numerical Combustion, SIAM, St. Petersburg (1991).
[14]J. R. Saylor, ''Differential diffusion in turbulent and oscillatory nonturbulent, water flows,'' Ph. D. Thesis, Yale University, 1993.
[15]G. K. Batchelor, ''Small-scale variation of convected quantities like temperature in turbulent fluid. Part 1. General discussion and the case of small conductivity,'' J. Fluid Mech. **5**, 113 (1959).
[16]J. A. Quinn, C. H. Lin, and J. L. Anderson, ''Measuring diffusion coefficients by Taylor's method of hydrodynamic stability,'' AIChE. J. **32**, 2028 (1986).
[17]E. L. Cussler, *Diffusion Mass Transfer in Fluid Systems* (Cambridge University Press, New York, 1984).
[18]J. R. Saylor, ''Photobleaching of disodium fluorescein in water,'' Exp. Fluids **18**, 445 (1995).
[19]K. R. Sreenivasan and C. Meneveau, ''The fractal facets of turbulents,'' J. Fluid Mech. **173**, 386 (1986).
[20]D. R. Dowling, ''The estimated scalar dissipation rate in gas-phase turbulent jets,'' Phys. Fluids A **3**, 2229 (1991).
[21]D. R. Dowling and P. E. Dimotakis, ''Similarity of the concentration field of gas-phase turbulent jets,'' J. Fluid Mech. **218**, 109 (1990).
[22]K. R. Sreenivasan and R. R. Prasad, ''New results on the fractal and multifractal structure of the large Schmidt number passive scalars in fully turbulent flows,'' Physica D **38**, 322 (1989).
[23]H. A. Becker, H. C. Hottel, and G. C. Williams, ''The nozzle-fluid concentration field of the round, turbulent, free jet,'' J. Fluid Mech. **30**, part 2, 285 (1967).
[24]M. B. Long, ''Multidimensional imaging in combusting flows by Lorenz-Mie, Rayleigh, and Raman Scattering,'' in *Instrumentation for Flows with Combustion*, edited by A. M. K. P. Taylor (Academic, London, 1993), p. 467.